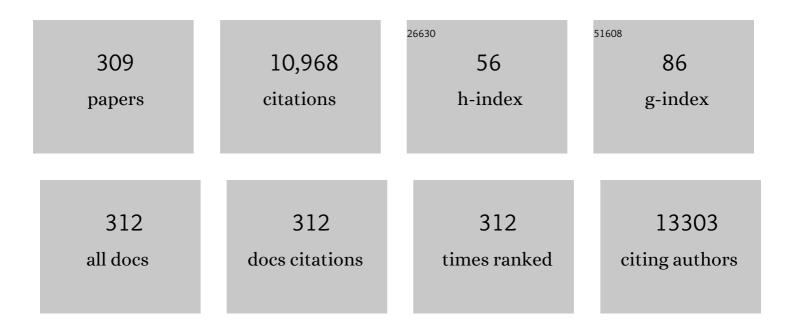
## Liang Zhen

List of Publications by Year in descending order

Source: https://exaly.com/author-pdf/555177/publications.pdf Version: 2024-02-01



LIANC THEN

#	Article	IF	CITATIONS
1	Formation of Uniform Fe <sub>3</sub> O <sub>4</sub> Hollow Spheres Organized by Ultrathin Nanosheets and Their Excellent Lithium Storage Properties. Advanced Materials, 2015, 27, 4097-4101.	21.0	396
2	Ternary Metal Phosphide with Tripleâ€Layered Structure as a Lowâ€Cost and Efficient Electrocatalyst for Bifunctional Water Splitting. Advanced Functional Materials, 2016, 26, 7644-7651.	14.9	389
3	Flow behavior and microstructures of superalloy 718 during high temperature deformation. Materials Science & Engineering A: Structural Materials: Properties, Microstructure and Processing, 2008, 497, 479-486.	5.6	227
4	Monodisperse SnS <sub>2</sub> Nanosheets for High-Performance Photocatalytic Hydrogen Generation. ACS Applied Materials & Interfaces, 2014, 6, 22370-22377.	8.0	216
5	Carrier Control of MoS <sub>2</sub> Nanoflakes by Functional Self-Assembled Monolayers. ACS Nano, 2013, 7, 7795-7804.	14.6	208
6	Microstructure evolution during dynamic recrystallization of hot deformed superalloy 718. Materials Science & Engineering A: Structural Materials: Properties, Microstructure and Processing, 2008, 486, 321-332.	5.6	179
7	Investigation of precipitation behavior and related hardening in AA 7055 aluminum alloy. Materials Science & Engineering A: Structural Materials: Properties, Microstructure and Processing, 2009, 500, 34-42.	5.6	162
8	Intrinsically Mn <sup>2+</sup> -Chelated Polydopamine Nanoparticles for Simultaneous Magnetic Resonance Imaging and Photothermal Ablation of Cancer Cells. ACS Applied Materials & Interfaces, 2015, 7, 16946-16952.	8.0	153
9	Photodiode-Like Behavior and Excellent Photoresponse of Vertical Si/Monolayer MoS2 Heterostructures. Scientific Reports, 2014, 4, 7186.	3.3	141
10	Deformation behavior and microstructure evolution of 7050 aluminum alloy during high temperature deformation. Materials Science & Engineering A: Structural Materials: Properties, Microstructure and Processing, 2008, 488, 64-71.	5.6	139
11	Sulfurizing-Induced Hollowing of Co <sub>9</sub> S <sub>8</sub> Microplates with Nanosheet Units for Highly Efficient Water Oxidation. ACS Applied Materials & Interfaces, 2017, 9, 11634-11641.	8.0	129
12	Surface potential and interlayer screening effects of few-layer MoS2 nanoflakes. Applied Physics Letters, 2013, 102, .	3.3	125
13	Microwave absorption properties of FeNi <sub>3</sub> submicrometre spheres and SiO <sub>2</sub> @FeNi <sub>3</sub> core–shell structures. Journal Physics D: Applied Physics, 2010, 43, 245003.	2.8	116
14	Carbon-Coated Nickel Phosphide Nanosheets as Efficient Dual-Electrocatalyst for Overall Water Splitting. ACS Applied Materials & Interfaces, 2016, 8, 27850-27858.	8.0	113
15	Precipitation behaviour of Al-Mg-Si alloys with high silicon content. Journal of Materials Science, 1997, 32, 1895-1902.	3.7	111
16	Co <sub>7</sub> Fe <sub>3</sub> and Co <sub>7</sub> Fe <sub>3</sub> @SiO <sub>2</sub> Nanospheres with Tunable Diameters for High-Performance Electromagnetic Wave Absorption. ACS Applied Materials & Interfaces, 2017, 9, 21933-21941.	8.0	109
17	Synthesis of Single-Crystalline Niobate Nanorods via Ion-Exchange Based on Molten-Salt Reaction. Journal of the American Chemical Society, 2007, 129, 15444-15445.	13.7	104
18	Synthesis and characterization of single-crystalline MnFe2O4 nanorods via a surfactant-free hydrothermal route. Journal of Magnetism and Magnetic Materials, 2008, 320, 2672-2675.	2.3	104

#	Article	IF	CITATIONS
19	Hot deformation behavior of delta-processed superalloy 718. Materials Science & Engineering A: Structural Materials: Properties, Microstructure and Processing, 2011, 528, 3218-3227.	5.6	101
20	Synthesis and Characterization of Single-Crystalline Alkali Titanate Nanowires. Journal of the American Chemical Society, 2005, 127, 11584-11585.	13.7	99
21	Room Temperature Synthesis of Hollow CdMoO4Microspheres by a Surfactant-Free Aqueous Solution Route. Journal of Physical Chemistry B, 2006, 110, 23154-23158.	2.6	97
22	Hot working characteristics and dynamic recrystallization of delta-processed superalloy 718. Journal of Alloys and Compounds, 2009, 474, 341-346.	5.5	97
23	Ageing behavior and stress corrosion cracking resistance of a non-isothermally aged Al–Zn–Mg–Cu alloy. Materials Science & Engineering A: Structural Materials: Properties, Microstructure and Processing, 2014, 605, 167-175.	5.6	97
24	Encapsulating MnO nanoparticles within foam-like carbon nanosheet matrix for fast and durable lithium storage. Nano Energy, 2018, 50, 675-684.	16.0	95
25	Crystallization kinetics and phase transformation of poly(vinylidene fluoride) films incorporated with functionalized baTiO <sub>3</sub> nanoparticles. Journal of Applied Polymer Science, 2013, 129, 2940-2949.	2.6	92
26	Bifunctional WC‣upported RuO <sub>2</sub> Nanoparticles for Robust Water Splitting in Acidic Media. Angewandte Chemie - International Edition, 2022, 61, .	13.8	89
27	Epitaxial Growth of Shape-Controlled Bi <sub>2</sub> Te <sub>3</sub> â^'Te Heterogeneous Nanostructures. Journal of the American Chemical Society, 2010, 132, 17316-17324.	13.7	87
28	Room Temperature Synthesis, Growth Mechanism, Photocatalytic and Photoluminescence Properties of Cadmium Molybdate Coreâ~'Shell Microspheres. Crystal Growth and Design, 2009, 9, 1558-1568.	3.0	86
29	Giant electrocaloric effect in BaZr0.2Ti0.8O3 thick film. Applied Physics Letters, 2014, 105, .	3.3	84
30	Microstructure characterization of 7050 aluminum alloy during dynamic recrystallization and dynamic recovery. Materials Characterization, 2008, 59, 1185-1189.	4.4	82
31	Phase Transition Induced Synthesis of Layered/Spinel Heterostructure with Enhanced Electrochemical Properties. Advanced Functional Materials, 2017, 27, 1604349.	14.9	80
32	Controlled Synthesis of Calcium Tungstate Hollow Microspheres via Ostwald Ripening and Their Photoluminescence Property. Journal of Physical Chemistry C, 2008, 112, 19390-19398.	3.1	79
33	Synthesis of hexagonal Fe microflakes with excellent microwave absorption performance. CrystEngComm, 2012, 14, 6827.	2.6	79
34	A study on graphitization of diamond in copper–diamond composite materials. Materials Letters, 2004, 58, 146-149.	2.6	77
35	Effect of electroactive phase transformation on electron structure and dielectric properties of uniaxial stretching poly(vinylidene fluoride) films. RSC Advances, 2013, 3, 23730.	3.6	76
36	Resonance-antiresonance electromagnetic behavior in a disordered dielectric composite. Applied Physics Letters, 2007, 90, 142907.	3.3	75

#	Article	IF	CITATIONS
37	Accelerated precipitation and growth of phases in an Al-Zn-Mg-Cu alloy processed by surface abrasion. Acta Materialia, 2017, 131, 233-245.	7.9	71
38	Synthesis, characterization and electromagnetic properties of Fe1â^'xCox alloy flower-like microparticles. Journal of Magnetism and Magnetic Materials, 2011, 323, 515-520.	2.3	70
39	DSC analyses of the precipitation behavior of two Al–Mg–Si alloys naturally aged for different times. Materials Letters, 1998, 37, 349-353.	2.6	69
40	Electromagnetic properties of FeNi alloy nanoparticles prepared by hydrogen-thermal reduction method. Journal of Applied Physics, 2008, 104, .	2.5	69
41	MOF-Derived Cu <sub>2</sub> O/Cu Nanospheres Anchored in Nitrogen-Doped Hollow Porous Carbon Framework for Increasing the Selectivity and Activity of Electrochemical CO <sub>2</sub> -to-Formate Conversion. ACS Applied Materials & Interfaces, 2020, 12, 7030-7037.	8.0	69
42	Room Temperature Synthesis of Hierarchical SrCO <sub>3</sub> Architectures by a Surfactant-Free Aqueous Solution Route. Crystal Growth and Design, 2008, 8, 1734-1740.	3.0	68
43	Construction of FeP Hollow Nanoparticles Densely Encapsulated in Carbon Nanosheet Frameworks for Efficient and Durable Electrocatalytic Hydrogen Production. Advanced Science, 2019, 6, 1801490.	11.2	68
44	Hydrothermal synthesis and characterization of single-crystalline Fe3O4 nanowires with high aspect ratio and uniformity. Materials Letters, 2007, 61, 3159-3162.	2.6	67
45	Glucose-Derived Carbonaceous Nanospheres for Photoacoustic Imaging and Photothermal Therapy. ACS Applied Materials & Interfaces, 2016, 8, 15904-15910.	8.0	67
46	NiSe <sub>2</sub> pyramids deposited on N-doped graphene encapsulated Ni foam for high-performance water oxidation. Journal of Materials Chemistry A, 2017, 5, 3981-3986.	10.3	67
47	Shape- and Size-Controlled Synthesis of Calcium Molybdate Doughnut-Shaped Microstructures. Journal of Physical Chemistry C, 2009, 113, 16414-16423.	3.1	66
48	The effect of pre-aging on microstructure and tensile properties of Al-Mg-Si alloys. Scripta Materialia, 1997, 36, 1089-1094.	5.2	65
49	Elastic properties of suspended black phosphorus nanosheets. Applied Physics Letters, 2016, 108, .	3.3	65
50	Internal Biasing in Relaxor Ferroelectric Polymer to Enhance the Electrocaloric Effect. Advanced Functional Materials, 2015, 25, 5134-5139.	14.9	64
51	In Situ Growth of Snâ€Doped Ni <sub>3</sub> S <sub>2</sub> Nanosheets on Ni Foam as Highâ€Performance Electrocatalyst for Hydrogen Evolution Reaction. ChemElectroChem, 2017, 4, 594-600.	3.4	64
52	The effect of Cu and Sc on the localized corrosion resistance of Al-Zn-Mg-X alloys. Journal of Alloys and Compounds, 2019, 799, 1-14.	5.5	63
53	Aqueous Solution Synthesis of Cd(OH)2 Hollow Microspheres via Ostwald Ripening and Their Conversion to CdO Hollow Microspheres. Journal of Physical Chemistry C, 2008, 112, 14360-14366.	3.1	62
54	Deformation localization and recrystallization in TC4 alloy under impact condition. Materials Science & Engineering A: Structural Materials: Properties, Microstructure and Processing, 2005, 395, 98-101.	5.6	60

#	Article	IF	CITATIONS
55	Hydrothermal synthesis of well-dispersed LiMnPO4 plates for lithium ion batteries cathode. Electrochimica Acta, 2013, 87, 303-308.	5.2	60
56	Molten salt synthesis of Na2Ti3O7 and Na2Ti6O13 one-dimensional nanostructures and their photocatalytic and humidity sensing properties. CrystEngComm, 2013, 15, 3448.	2.6	60
57	Stress relaxation behavior of an Al–Zn–Mg–Cu alloy in simulated age-forming process. Journal of Materials Processing Technology, 2014, 214, 775-783.	6.3	59
58	Understanding the phase transitions in spinel-layered-rock salt system: Criterion for the rational design of LLO/spinel nanocomposites. Nano Energy, 2017, 40, 566-575.	16.0	58
59	Liquid Exfoliation of Colloidal Rhenium Disulfide Nanosheets as a Multifunctional Theranostic Agent for In Vivo Photoacoustic/CT Imaging and Photothermal Therapy. Small, 2018, 14, e1703789.	10.0	58
60	Characterization of adiabatic shear bands in AM60B magnesium alloy under ballistic impact. Materials Characterization, 2011, 62, 496-502.	4.4	56
61	Solvothermal synthesis of Bi2WO6 hollow structures with excellent visible-light photocatalytic properties. Materials Letters, 2013, 95, 117-120.	2.6	56
62	Tuning the Excitonic States in MoS <sub>2</sub> /Graphene van der Waals Heterostructures via Electrochemical Gating. Advanced Functional Materials, 2016, 26, 293-302.	14.9	56
63	Tuning the pore structure of porous tin foam electrodes for enhanced electrochemical reduction of carbon dioxide to formate. Chemical Engineering Journal, 2019, 375, 122024.	12.7	56
64	Enhancement of strength and electrical conductivity for a dilute Al-Sc-Zr alloy via heat treatments and cold drawing. Journal of Materials Science and Technology, 2019, 35, 962-971.	10.7	56
65	Aqueous Solution Synthesis of CaF <sub>2</sub> Hollow Microspheres via the Ostwald Ripening Process at Room Temperature. ACS Applied Materials & Interfaces, 2009, 1, 780-788.	8.0	55
66	Effect of Cu Content and Aging Conditions on Pitting Corrosion Damage of 7xxx Series Aluminum Alloys. Journal of the Electrochemical Society, 2015, 162, C150-C160.	2.9	55
67	Ternary SnS2–xSex Alloys Nanosheets and Nanosheet Assemblies with Tunable Chemical Compositions and Band Gaps for Photodetector Applications. Scientific Reports, 2015, 5, 17109.	3.3	54
68	Highly reversible oxygen redox in layered compounds enabled by surface polyanions. Nature Communications, 2020, 11, 3411.	12.8	54
69	Facile synthesis of porous Cu-Sn alloy electrode with prior selectivity of formate in a wide potential range for CO2 electrochemical reduction. Applied Catalysis B: Environmental, 2021, 292, 120119.	20.2	54
70	Preparation of CoFe alloy nanoparticles with tunable electromagnetic wave absorption performance. Journal of Magnetism and Magnetic Materials, 2009, 321, 3702-3705.	2.3	53
71	Self-organized sheaf-like Fe <sub>3</sub> O <sub>4</sub> /C hierarchical microrods with superior lithium storage properties. Nanoscale, 2015, 7, 4411-4414.	5.6	53
72	Microstructure evolution of adiabatic shear bands in AM60B magnesium alloy under ballistic impact. Materials Science & Engineering A: Structural Materials: Properties, Microstructure and Processing, 2010, 527, 5728-5733.	5.6	52

#	Article	IF	CITATIONS
73	Microstructures and mechanical properties of age-formed 7050 aluminum alloy. Materials Science & Engineering A: Structural Materials: Properties, Microstructure and Processing, 2012, 539, 115-123.	5.6	52
74	Epitaxial Growth of 1D Atomic Chain Based Se Nanoplates on Monolayer ReS <sub>2</sub> for Highâ€Performance Photodetectors. Advanced Functional Materials, 2018, 28, 1806254.	14.9	52
75	Biocompatible Fe3+–TA coordination complex with high photothermal conversion efficiency for ablation of cancer cells. Colloids and Surfaces B: Biointerfaces, 2018, 167, 183-190.	5.0	50
76	High photocatalytic activity and photoluminescence property of hollow CdMoO4 microspheres. Scripta Materialia, 2008, 58, 461-464.	5.2	49
77	A facile hydrothermal route to the large-scale synthesis of CoWO4 nanorods. Materials Letters, 2008, 62, 1740-1742.	2.6	49
78	Synthesis and microwave electromagnetic properties of CoFe alloy nanoflakes prepared with hydrogen-thermal reduction method. Journal of Applied Physics, 2009, 106, .	2.5	49
79	Dopamine-Induced Formation of Ultrasmall Few-Layer MoS <sub>2</sub> Homogeneously Embedded in N-Doped Carbon Framework for Enhanced Lithium-Ion Storage. ACS Applied Materials & Interfaces, 2016, 8, 33741-33748.	8.0	49
80	Non-isothermal ageing of an Al–8Zn–2Mg–2Cu alloy for enhanced properties. Journal of Materials Processing Technology, 2016, 227, 110-116.	6.3	49
81	Ca(II) doped β-In2S3 hierarchical structures for photocatalytic hydrogen generation and organic dye degradation under visible light irradiation. Journal of Colloid and Interface Science, 2017, 491, 230-237.	9.4	49
82	Distribution characterization of boundary misorientation angle of 7050 aluminum alloy after high-temperature compression. Journal of Materials Processing Technology, 2009, 209, 754-761.	6.3	47
83	Electrical and photocatalytic properties of Na2Ti6O13 nanobelts prepared by molten salt synthesis. Applied Surface Science, 2009, 255, 4149-4152.	6.1	47
84	Electric Field Tunable Interlayer Relaxation Process and Interlayer Coupling in WSe <sub>2</sub> /Graphene Heterostructures. Advanced Functional Materials, 2016, 26, 4319-4328.	14.9	47
85	Strong dual-frequency electromagnetic absorption in Ku-band of C@FeNi3 core/shell structured microchains with negative permeability. Journal of Magnetism and Magnetic Materials, 2014, 349, 159-164.	2.3	46
86	Constructing yolk-shell MnO@C nanodiscs through a carbothermal reduction process for highly stable lithium storage. Chemical Engineering Journal, 2018, 336, 427-435.	12.7	45
87	Fractal growth of single-crystal α-Fe2O3: From dendritic micro-pines to hexagonal micro-snowflakes. Materials Letters, 2008, 62, 739-742.	2.6	44
88	Sulfur vacancies promoting Fe-doped Ni <sub>3</sub> S <sub>2</sub> nanopyramid arrays as efficient bifunctional electrocatalysts for overall water splitting. Sustainable Energy and Fuels, 2020, 4, 3326-3333.	4.9	44
89	Carbon-coated CoFe–CoFe <sub>2</sub> O <sub>4</sub> composite particles with high and dual-band electromagnetic wave absorbing properties. Nanotechnology, 2018, 29, 305604.	2.6	43
90	Influence of Mg content on ageing precipitation behavior of Al-Cu-Li-x alloys. Materials Science & Engineering A: Structural Materials: Properties, Microstructure and Processing, 2019, 742, 138-149.	5.6	43

#	Article	IF	CITATIONS
91	Anisotropic Signal Processing with Trigonal Selenium Nanosheet Synaptic Transistors. ACS Nano, 2020, 14, 10018-10026.	14.6	43
92	Tensile deformation behavior of superalloy 718 at elevated temperatures. Journal of Alloys and Compounds, 2009, 471, 331-335.	5.5	42
93	Tetradecylphosphonic acid modified BaTiO3 nanoparticles and its nanocomposite. Colloids and Surfaces A: Physicochemical and Engineering Aspects, 2013, 427, 19-25.	4.7	42
94	Deformation and fracture behavior of two Al-Mg-Si alloys. Metallurgical and Materials Transactions A: Physical Metallurgy and Materials Science, 1997, 28, 1489-1497.	2.2	41
95	A pressure sensor based on the orientational dependence of plasmonic properties of gold nanorods. Nanoscale, 2015, 7, 14483-14488.	5.6	41
96	Microwave absorption properties of FeSi flaky particles prepared via a ball-milling process. Journal of Magnetism and Magnetic Materials, 2015, 395, 152-158.	2.3	41
97	Particle-stimulated nucleation and recrystallization texture initiated by coarsened Al2CuLi phase in Al–Cu–Li alloy. Journal of Materials Research and Technology, 2021, 10, 643-650.	5.8	41
98	Synthesis of Fe–ferrite composite nanotubes with excellent microwave absorption performance. CrystEngComm, 2011, 13, 6839.	2.6	40
99	Formation of CdMoO4 porous hollow nanospheres via a self-assembly accompanied with Ostwald ripening process and their photocatalytic performance. CrystEngComm, 2013, 15, 8014.	2.6	39
100	Development of La0.6Sr0.4Co0.2Fe0.8O3â~ʾĨ´ cathode with an improved stability via La0.8Sr0.2MnO3-film impregnation. International Journal of Hydrogen Energy, 2013, 38, 5375-5382.	7.1	39
101	In-situ growth of graphene decorated Ni3S2 pyramids on Ni foam for high-performance overall water splitting. Applied Surface Science, 2019, 465, 772-779.	6.1	39
102	Synthesis of Fe/SiO2 composite particles and their superior electromagnetic properties in microwave band. Materials Letters, 2010, 64, 57-60.	2.6	38
103	Microstructure and magnetic properties of SiC/Co composite particles prepared by electroless plating. Surface and Coatings Technology, 2006, 201, 3139-3146.	4.8	37
104	Effects of precipitates on fatigue crack growth rate of AA 7055 aluminum alloy. Transactions of Nonferrous Metals Society of China, 2010, 20, 2209-2214.	4.2	37
105	Formation of FeMoO4 hollow microspheres via a chemical conversion-induced Ostwald ripening process. CrystEngComm, 2012, 14, 7025.	2.6	37
106	Mechanism of Localized Breakdown of 7000 Series Aluminum Alloys. Journal of the Electrochemical Society, 2013, 160, C493-C502.	2.9	37
107	Effects of coarse Al2CuLi phase on the hot deformation behavior of Al–Li alloy. Journal of Alloys and Compounds, 2020, 815, 152469.	5.5	37
108	Ultrathin Co9S8 nanosheets vertically aligned on N,S/rGO for low voltage electrolytic water in alkaline media. Scientific Reports, 2019, 9, 1951.	3.3	36

#	Article	IF	CITATIONS
109	Deformed microstructure evolution in AM60B Mg alloy under hypervelocity impact at a velocity of 5kmsâ^'1. Materials & Design, 2010, 31, 3708-3715.	5.1	35
110	Eu3+-doped CdMoO4 red phosphor synthesized through an aqueous solution route at room temperature. Journal of Alloys and Compounds, 2012, 529, 17-20.	5.5	35
111	Low temperature electrochemical performance of β-Li V2O5 cathode for lithium-ion batteries. Electrochimica Acta, 2015, 169, 440-446.	5.2	35
112	Work function modulation of bilayer MoS2 nanoflake by backgate electric field effect. Applied Physics Letters, 2013, 103, .	3.3	34
113	Synthesis of Bi2WO6 hierarchical structures constructed by porous nanoplates and their associated photocatalytic properties under visible light irradiation. Ceramics International, 2014, 40, 11689-11698.	4.8	34
114	Hybrid dual-channel phototransistor based on 1D t-Se and 2D ReS2 mixed-dimensional heterostructures. Nano Research, 2019, 12, 669-674.	10.4	34
115	Micro-damage behaviors of Al–6Mg alloy impacted by projectiles with velocities of 1–3.2km/s. Materials Science & Engineering A: Structural Materials: Properties, Microstructure and Processing, 2005, 391, 354-366.	5.6	33
116	Deformed microstructure and mechanical properties of AM60B magnesium alloy under hypervelocity impact at a velocity of 4kmsâ^'1. Materials Science & Engineering A: Structural Materials: Properties, Microstructure and Processing, 2010, 527, 3323-3328.	5.6	33
117	Synthesis of LiMnPO4 microspheres assembled by plates, wedges and prisms with different crystallographic orientations and their electrochemical performance. CrystEngComm, 2012, 14, 6412.	2.6	33
118	Segregation of the major alloying elements to Al3(Sc,Zr) precipitates in an Al–Zn–Mg–Cu–Sc–Zr alloy. Materials Characterization, 2019, 157, 109898.	4.4	33
119	Microstructure and magnetic properties of Fe–25Cr–12Co–1Si alloy thermo-magnetically treated in intense magnetic field. Journal of Magnetism and Magnetic Materials, 2004, 283, 231-237.	2.3	32
120	Chelate-induced formation of Li <sub>2</sub> MnSiO <sub>4</sub> nanorods as a high capacity cathode material for Li-ion batteries. Journal of Materials Chemistry A, 2016, 4, 9447-9454.	10.3	32
121	Correlation between precipitates evolution and mechanical properties of Al-Sc-Zr alloy with Er additions. Journal of Materials Science and Technology, 2022, 99, 61-72.	10.7	32
122	FeNi3/indium tin oxide (ITO) composite nanoparticles with excellent microwave absorption performance and low infrared emissivity. Materials Science and Engineering B: Solid-State Materials for Advanced Technology, 2013, 178, 225-230.	3.5	31
123	Photoresponse Enhancement in Monolayer ReS <sub>2</sub> Phototransistor Decorated with CdSe–CdS–ZnS Quantum Dots. ACS Applied Materials & Interfaces, 2017, 9, 39456-39463.	8.0	31
124	Rational Construction of Uniform CoNi-Based Core-Shell Microspheres with Tunable Electromagnetic Wave Absorption Properties. Scientific Reports, 2018, 8, 3196.	3.3	31
125	Natural Humicâ€Acidâ€Based Phototheranostic Agent. Advanced Healthcare Materials, 2018, 7, e1701202.	7.6	31
126	Reviving reversible anion redox in 3d-transition-metal Li rich oxides by introducing surface defects. Nano Energy, 2020, 71, 104644.	16.0	31

#	Article	IF	CITATIONS
127	Through-thickness texture gradient in AA 7055 aluminum alloy. Materials Letters, 2008, 62, 88-90.	2.6	30
128	Chemical Vapor Deposition Growth of Degenerate p-Type Mo-Doped ReS <sub>2</sub> Films and Their Homojunction. ACS Applied Materials & Interfaces, 2017, 9, 15583-15591.	8.0	30
129	Minimization of Residual Stress in an Al-Cu Alloy Forged Plate by Different Heat Treatments. Journal of Materials Engineering and Performance, 2015, 24, 2256-2265.	2.5	29
130	van der Waals epitaxy of large-area continuous ReS <sub>2</sub> films on mica substrate. RSC Advances, 2017, 7, 24188-24194.	3.6	29
131	High capacity and enhanced structural reversibility of $\hat{l}^2$ -LixV2O5 nanorods as the lithium battery cathode. Journal of Materials Chemistry A, 2013, 1, 5361.	10.3	28
132	Solvothermal synthesis of orthorhombic Sb <sub>2</sub> WO <sub>6</sub> hierarchical structures and their visible-light-driven photocatalytic activity. Dalton Transactions, 2014, 43, 8439-8445.	3.3	27
133	PEGylated Tantalum Nanoparticles: A Metallic Photoacoustic Contrast Agent for Multiwavelength Imaging of Tumors. Small, 2019, 15, e1903596.	10.0	27
134	Development of microstructures and texture during cold rolling in AA 7055 aluminum alloy. Materials Science & Engineering A: Structural Materials: Properties, Microstructure and Processing, 2009, 504, 55-63.	5.6	26
135	Large-scale synthesis of single-crystalline KNb3O8 nanobelts via a simple molten salt method. Ceramics International, 2010, 36, 679-682.	4.8	25
136	Electromagnetic properties of flake-shaped Fe–Si alloy particles prepared by ball milling. Journal of Magnetism and Magnetic Materials, 2014, 368, 295-299.	2.3	25
137	Solution-phase synthesis of γ-In <sub>2</sub> Se <sub>3</sub> nanoparticles for highly efficient photocatalytic hydrogen generation under simulated sunlight irradiation. RSC Advances, 2016, 6, 106671-106675.	3.6	25
138	Improvement on electromagnetic absorbing performance of Al18B4O33w/Co composite particles through heat treatment. Scripta Materialia, 2008, 59, 967-970.	5.2	24
139	Fractal Analysis of Disordered Conductor–Insulator Composites with Different Conductor Backbone Structures near Percolation Threshold. Journal of Physical Chemistry C, 2012, 116, 19517-19525.	3.1	24
140	Ferroelectric resistive switching behavior in two-dimensional materials/BiFeO <sub>3</sub> hetero-junctions. Nanoscale, 2018, 10, 23080-23086.	5.6	24
141	Selective CO <sub>2</sub> -to-formate electrochemical conversion with core–shell structured Cu <sub>2</sub> O/Cu@C composites immobilized on nitrogen-doped graphene sheets. Journal of Materials Chemistry A, 2020, 8, 18302-18309.	10.3	24
142	Shape-controlled synthesis of zinc phosphate nanostructures by an aqueous solution route at room temperature. Materials Letters, 2012, 82, 26-28.	2.6	23
143	Sandwich-like cobalt/reduced graphene oxide/cobalt composite structure presenting synergetic electromagnetic loss effect. Journal of Colloid and Interface Science, 2020, 561, 687-695.	9.4	23
144	Macro- and microdamage behaviors of the 30CrMnSiA steel impacted by hypervelocity projectiles. Materials Science & Engineering A: Structural Materials: Properties, Microstructure and Processing, 2000, 282, 177-182.	5.6	22

#	Article	IF	CITATIONS
145	Disket-Nanorings of K <sub>2</sub> Ti <sub>6</sub> O <sub>13</sub> Formed by Self-Spiraling of a Nanobelt. Journal of Physical Chemistry C, 2008, 112, 7547-7551.	3.1	22
146	Portevin-Le Chatelier effect in Al-Zn-Mg-Cu-Zr aluminum alloy. Transactions of Nonferrous Metals Society of China, 2009, 19, 1071-1075.	4.2	22
147	Structural transformations in Li <sub>2</sub> MnSiO <sub>4</sub> : evidence that a Li intercalation material can reversibly cycle through a disordered phase. Journal of Materials Chemistry A, 2017, 5, 16722-16731.	10.3	22
148	Cu <sub>2</sub> O/Cu Cermet as a Candidate Inert Anode for Al Production. International Journal of Applied Ceramic Technology, 2007, 4, 453-462.	2.1	21
149	A facile molten salt route to K2Nb8O21 nanoribbons. Ceramics International, 2008, 34, 435-437.	4.8	21
150	Conductivity critical exponents lower than the universal value in continuum percolation systems. Journal of Physics Condensed Matter, 2008, 20, 395235.	1.8	21
151	Phase field simulation of microstructure evolution in Fe–Cr–Co alloy during thermal magnetic treatment and step aging. Journal of Magnetism and Magnetic Materials, 2010, 322, 987-995.	2.3	21
152	Microstructure evolution in abrasion-induced surface layer on an Al–Zn–Mg–Cu alloy. Materials Characterization, 2014, 98, 18-25.	4.4	21
153	Electrochemical reduction of carbon dioxide to formate via nano-prism assembled CuO microspheres. Chemosphere, 2019, 237, 124527.	8.2	21
154	Electrochemical Intercalation in Atomically Thin van der Waals Materials for Structural Phase Transition and Device Applications. Advanced Materials, 2021, 33, e2000581.	21.0	21
155	Synthesis of CoFe/Al2O3 composite nanoparticles as the impedance matching layer of wideband multilayer absorber. Journal of Applied Physics, 2011, 109, 07A332.	2.5	20
156	Experimental study on modulated structure in Alnico alloys under high magnetic field and comparison with phase-field simulation. Journal of Magnetism and Magnetic Materials, 2013, 348, 27-32.	2.3	20
157	Large-scale Synthesis of SrCrO4Nanowires and PbCrO4Nanorods by a Solution-phase Method at Room Temperature. Chemistry Letters, 2006, 35, 268-269.	1.3	19
158	Effect of γ-ray irradiation on the magnetic properties of NdFeB and Fe–Cr–Co permanent magnets. Journal of Magnetism and Magnetic Materials, 2006, 302, 156-159.	2.3	18
159	Microstructure evolution of cobalt coating electroless plated on SiC whisker during electroless plating and heat treatment. Surface and Coatings Technology, 2007, 201, 6059-6062.	4.8	18
160	Evolution of modulated structure in Fe–Cr–Co alloy during isothermal ageing with different external magnetic field conditions. Journal of Magnetism and Magnetic Materials, 2007, 312, 342-346.	2.3	18
161	Characterization of the deformed microstructure in 1Cr18NiTi stainless steel under ballistic impact. Materials Science & Engineering A: Structural Materials: Properties, Microstructure and Processing, 2008, 489, 213-219.	5.6	18
162	Hydrothermal synthesis, magnetic and electromagnetic properties of hexagonal Fe3O4 microplates. Journal of Magnetism and Magnetic Materials, 2014, 361, 161-165.	2.3	18

#	Article	IF	CITATIONS
163	Synthesis of self-stacked CuFe <sub>2</sub> O <sub>4</sub> –Fe <sub>2</sub> O <sub>3</sub> porous nanosheets as a high performance Li-ion battery anode. Journal of Materials Chemistry A, 2014, 2, 19330-19337.	10.3	18
164	Study of Î <sup>3</sup> -ray irradiation effect on permanent magnets. Journal of Applied Physics, 2008, 103, 07E136.	2.5	17
165	Co/SiO2 composite particles with high electromagnetic wave absorbing performance and weather resistance. Journal of Magnetism and Magnetic Materials, 2013, 334, 111-118.	2.3	17
166	Effect of Surface Roughness on Breakdown Behavior of Al-Zn-Mg-Cu Alloy. Journal of the Electrochemical Society, 2014, 161, C433-C440.	2.9	17
167	Self-standing flexible cathode of V2O5 nanobelts with high cycling stability for lithium-ion batteries. Ceramics International, 2016, 42, 14595-14600.	4.8	17
168	Microstructure Evolution and the Resulted Influence on Localized Corrosion in Al-Zn-Mg-Cu Alloy during Non-Isothermal Ageing. Materials, 2018, 11, 720.	2.9	17
169	Effects of interfacial wettability on arc erosion behavior of Zn2SnO4/Cu electrical contacts. Journal of Materials Science and Technology, 2022, 109, 64-75.	10.7	17
170	In situ tensile deformation and fracture behavior of Ti–24Al–14Nb–3V–0.5Mo alloy with various microstructures. Intermetallics, 2004, 12, 43-53.	3.9	16
171	Magnetic anisotropy in Fe-25Cr-12Co-1Si alloy induced by external magnetic field. Transactions of Nonferrous Metals Society of China, 2007, 17, 346-350.	4.2	16
172	Thermal expansion behavior of Cu/Cu2O cermets with different Cu structures. Ceramics International, 2009, 35, 2803-2807.	4.8	16
173	The influence of Fe content on the magnetic and electromagnetic characteristics for Fex(CoNi)1â^'x ternary alloy nanoparticles. Journal of Applied Physics, 2011, 109, 07A320.	2.5	16
174	The influence of hollow structure on the magnetic characteristics for Fe3O4 submicron spheres. Journal of Applied Physics, 2011, 109, 07B535.	2.5	16
175	Effect of ageâ€forming on corrosion properties of an Alï£įZnï£įMgï£įCu alloy. Materials and Corrosion - Werkstoffe Und Korrosion, 2014, 65, 670-677.	1.5	16
176	Electrochemical Lithium Insertion Behavior of <i>β</i> -Li <i><sub>x</sub></i> V <sub>2</sub> O <sub>5</sub> (0 < <i>x</i> â‰\$) as the Cathode Material for Secondary Lithium Batteries. Journal of the Electrochemical Society, 2014, 161, A75-A83.	2.9	16
177	Air arc erosion behavior of CuZr/Zn2SnO4 electrical contact materials. Journal of Alloys and Compounds, 2018, 743, 697-706.	5.5	16
178	TEM observation of the interface in a Ti3Al-Nb alloy. Materials Letters, 1997, 32, 319-323.	2.6	15
179	Study of deformed microstructures near the impact crater in pure copper targets. Materials Science & Engineering A: Structural Materials: Properties, Microstructure and Processing, 2004, 384, 12-18.	5.6	15
180	Dielectric and electrocaloric responses of Ba(Zr <sub>0.2</sub> Ti <sub>0.8</sub> )O <sub>3</sub> bulk ceramics and thick films with sintering aids. IEEE Transactions on Dielectrics and Electrical Insulation, 2015, 22, 1501-1505.	2.9	15

#	Article	IF	CITATIONS
181	Large-scale synthesis and characterization of fan-shaped rutile TiO2 nanostructures. Materials Letters, 2008, 62, 3404-3406.	2.6	14
182	Microstructure evolution and electromagnetic properties improvement of Al18B4O33w/Co composite powders through heat-treatment. Journal of Magnetism and Magnetic Materials, 2009, 321, 1290-1294.	2.3	14
183	Synthesis and formation process of SrSO <sub>4</sub> sisal-like hierarchical structures at room temperature. CrystEngComm, 2011, 13, 620-625.	2.6	14
184	Electromagnetic properties of Co flaky particles prepared via ball-milling method. Journal of Magnetism and Magnetic Materials, 2016, 416, 53-60.	2.3	14
185	Spinodal decomposition in Fe–25Cr–12Co–1Si alloy under a 100kOe magnetic field. Journal of Magnetism and Magnetic Materials, 2006, 306, 69-72.	2.3	13
186	Microstructural characterization of single-crystalline potassium hollandite nanowires. Materials Characterization, 2008, 59, 1805-1808.	4.4	13
187	Strain rate sensitivity of a high strain rate superplastic TiNp/2014 Al composite. Journal of Materials Processing Technology, 2010, 210, 734-740.	6.3	13
188	Effect of electron irradiation on electroactive phase and dielectric properties of PVDF films. RSC Advances, 2014, 4, 13525-13532.	3.6	13
189	Highly localized shear deformation in a Mg–Al–Mn alloy subjected to ballistic impact. Vacuum, 2019, 169, 108868.	3.5	13
190	Transformed shearing bands in strongly impact loaded 30CrMnSiA steel. Journal of Materials Science Letters, 1998, 17, 391-393.	0.5	12
191	Electrical Conductivity of Inhomogeneous Cu2O-10CuAlO2-xCu Cermets. Journal of the American Ceramic Society, 2005, 88, 2589-2593.	3.8	12
192	Numerical Simulation of Residual Stress in an Al-Cu Alloy Block During Quenching and Aging. Journal of Materials Engineering and Performance, 2015, 24, 4928-4940.	2.5	12
193	Mechanistic insights into interfaces and nitrogen vacancies in cobalt hydroxide/tungsten nitride catalysts to enhance alkaline hydrogen evolution. Journal of Materials Chemistry A, 2021, 9, 11323-11330.	10.3	12
194	Tuning the Energy Storage Efficiency in PVDF Nanocomposites Incorporated with Crumpled Core–Shell BaTiO <sub>3</sub> @Graphene Oxide Nanoparticles. ACS Applied Energy Materials, 2021, 4, 9553-9562.	5.1	12
195	Mechanical Anisotropy in Two-Dimensional Selenium Atomic Layers. Nano Letters, 2021, 21, 8043-8050.	9.1	12
196	Correlation between Structural Evolution and Device Performance of CH3NH3PbI3 Solar Cells under Proton Irradiation. ACS Applied Energy Materials, 0, , .	5.1	12
197	Room temperature synthesis of BaCrO4 nanoplates through a NaCl-assisted aqueous solution method. Materials Letters, 2007, 61, 3146-3149.	2.6	11
198	Electrical and microwave dielectric properties of K2Nb8O21 microwires. Ceramics International, 2009, 35, 3021-3025.	4.8	11

#	Article	IF	CITATIONS
199	Superparamagnetic nickel ferrite colloidal spheres for constructing magnetically responsive photonic crystals. Materials Letters, 2012, 81, 62-64.	2.6	11
200	Exploring Cu2O/Cu cermet as a partially inert anode to produce aluminum in a sustainable way. Journal of Alloys and Compounds, 2014, 610, 214-223.	5.5	11
201	Thickness-controllable coating of SiO2 on Co microspheres with tunable electromagnetic properties and enhanced oxidation resistance. RSC Advances, 2016, 6, 107653-107658.	3.6	11
202	Effects of dopants on the adhesion and electronic structure of a SnO <sub>2</sub> /Cu interface: a first-principles study. Physical Chemistry Chemical Physics, 2018, 20, 15618-15625.	2.8	11
203	Controlled Movement of a Smart Miniature Submarine at Various Interfaces. ACS Applied Materials & Interfaces, 2018, 10, 24899-24904.	8.0	11
204	Microstructure evolution of polyimide films induced by electron beam irradiation-load coupling treatment. Polymer Degradation and Stability, 2018, 155, 230-237.	5.8	11
205	Texture evolution and recrystallization mechanism in a Mg–3Al–1Zn alloy under ballistic impact. Journal of Alloys and Compounds, 2020, 816, 152599.	5.5	11
206	Bifunctional WCâ€Supported RuO <sub>2</sub> Nanoparticles for Robust Water Splitting in Acidic Media. Angewandte Chemie, 2022, 134, .	2.0	11
207	Single-crystalline PbCrO4 nanorods: Room temperature, surfactant free synthesis, characterization and optical property. Journal of Crystal Growth, 2007, 299, 86-93.	1.5	10
208	Magnetic microstructures of a high coercivity Nd–Fe–B sintered magnet in remanent and incomplete thermal demagnetization states. Journal of Magnetism and Magnetic Materials, 2010, 322, 3720-3723.	2.3	10
209	Thermal conductivity determination of conductor/insulator composites by fractal: Geometrical tortuosity and percolation. Composites Part B: Engineering, 2016, 92, 377-383.	12.0	10
210	Solvothermal Synthesis of Bi2O2CO3Nanoplates for Efficient Photodegradation of RhB and Phenol under Simulated Solar Light Irradiation. Bulletin of the Korean Chemical Society, 2014, 35, 2935-2940.	1.9	10
211	Deformation and fracture behavior of a RSP Al–Li alloy. Materials Science & Engineering A: Structural Materials: Properties, Microstructure and Processing, 2002, 336, 135-142.	5.6	9
212	Investigation on Dynamic Recrystallization Behavior in Hot Deformed Superalloy Inconel 718. Materials Science Forum, 2007, 546-549, 1297-1300.	0.3	9
213	Relationship between boundary misorientation angle and true strain during high temperature deformation of 7050 aluminum alloy. Transactions of Nonferrous Metals Society of China, 2008, 18, 795-798.	4.2	9
214	Influence of annealing on the structure and ferroelectric properties of Sr0.13Na0.37Bi0.50TiO3 thin films prepared by metalorganic solution deposition. Journal of Alloys and Compounds, 2010, 504, 155-158.	5.5	9
215	Effects of proton irradiation on structure of NdFeB permanent magnets studied by X-ray diffraction and X-ray absorption fine structure. Journal of Magnetism and Magnetic Materials, 2011, 323, 4-6.	2.3	9
216	Colloidal synthesis and formation mechanism of calcium molybdate notched microspheres. CrystEngComm, 2014, 16, 2598.	2.6	9

#	Article	IF	CITATIONS
217	Effect of Annealing Temperatures and Time on Structural Evolution and Dielectric Properties of PVDF Films. Polymers and Polymer Composites, 2016, 24, 167-172.	1.9	9
218	Electrochemical behavior and structural stability of LiV3O8 microrods as cathode for lithium-ion batteries. Ceramics International, 2016, 42, 18747-18755.	4.8	9
219	In situ soft-chemistry synthesis of β-Na <sub>0.33</sub> V <sub>2</sub> O <sub>5</sub> nanorods as high-performance cathode for lithium-ion batteries. RSC Advances, 2016, 6, 105833-105839.	3.6	9
220	Solvothermal Synthesis of <scp>InOOH</scp> Nanospheres with Enhanced Photocatalytic Activity. Bulletin of the Korean Chemical Society, 2016, 37, 522-528.	1.9	9
221	Designing Co7Fe3@TiO2 Core–Shell Nanospheres for Electromagnetic Wave Absorption in S and C Bands. Electronic Materials Letters, 2020, 16, 413-423.	2.2	9
222	Tailoring the Energy Funneling across the Interface in InSe/MoS <sub>2</sub> Heterostructures by Electrostatic Gating and Strain Engineering. Advanced Optical Materials, 2021, 9, 2100438.	7.3	9
223	Strain engineering of quasi-1D layered TiS3 nanosheets toward giant anisotropic Raman and piezoresistance responses. Applied Physics Letters, 2021, 119, .	3.3	9
224	2D Indium Phosphorus Sulfide (In <sub>2</sub> P <sub>3</sub> S <sub>9</sub> ): An Emerging van der Waals Highâ€ <i>k</i> Dielectrics. Small, 2022, 18, e2104401.	10.0	9
225	Environmentally Friendly Aqueous Solution Synthesis of Hierarchical CaWO <sub>4</sub> Microspheres at Room Temperature. Journal of Nanoscience and Nanotechnology, 2008, 8, 1288-1294.	0.9	8
226	Preparation and characterization of Ca0.18Na0.32Bi0.50TiO3 ferroelectric thin films by metalorganic solution deposition. Journal of Alloys and Compounds, 2010, 489, 136-139.	5.5	8
227	Single-crystal Na2Ti6O13 nanorings formed by self-coiling of a nanobelt. CrystEngComm, 2011, 13, 2674.	2.6	8
228	Synthesis of Zn(II)-Doped Magnetite Leaf-Like Nanorings for Efficient Electromagnetic Wave Absorption. Scientific Reports, 2017, 7, 45480.	3.3	8
229	Hierarchical Mn <sub>3</sub> O <sub>4</sub> Microplates Composed of Stacking Porous Nanosheets for Highâ€Performance Lithium Storage. ChemElectroChem, 2017, 4, 2703-2708.	3.4	8
230	Salt-templated synthesis of Co9S8 nanoparticles anchored on N, S co-doped carbon nanosheets towards high-performance water oxidation. Journal of Electroanalytical Chemistry, 2019, 835, 67-72.	3.8	8
231	Selfâ€Assembly of 2D Nanosheets into 1D Nanostructures for Sensing NO 2. Small Structures, 2021, 2, 2100067.	12.0	8
232	Effects of proton irradiation on electronic structure of NdFeB permanent magnets. Nuclear Instruments & Methods in Physics Research B, 2009, 267, 3084-3086.	1.4	7
233	Crystal plasticity simulation of polycrystalline aluminum and the effect of mesh refinement on mechanical responses. Materials Science & Engineering A: Structural Materials: Properties, Microstructure and Processing, 2011, 528, 6673-6679.	5.6	7
234	Topochemical synthesis and magnetic properties of BaFe12O19 nanorods using α-FeOOH nanowires as templates. Ceramics International, 2014, 40, 8593-8597.	4.8	7

#	Article	IF	CITATIONS
235	Mechanical properties of cermet composites with various geometrical tortuosity of metal phase: Fractal characterization. Materials Science & Engineering A: Structural Materials: Properties, Microstructure and Processing, 2014, 607, 236-244.	5.6	7
236	Self-supported construction of 3D CdMoO <sub>4</sub> hierarchical structures from nanoplates with enhanced photocatalytic properties. RSC Advances, 2014, 4, 38527-38534.	3.6	7
237	Sodium chloride induced formation of square-shaped cadmium molybdate nanoplates. Materials Letters, 2014, 131, 292-294.	2.6	7
238	Effects of long-term natural aging on the altered surface layer on an Al-Zn-Mg-Cu alloy and on corrosion properties. Electrochimica Acta, 2018, 266, 34-42.	5.2	7
239	Folded sheet resonators that aim at low frequency attenuation of surface elastic waves in solids. Journal of Applied Physics, 2020, 127, 164904.	2.5	7
240	Lowering the Contact Barriers of 2D Organic F <sub>16</sub> CuPc Fieldâ€Effect Transistors by Introducing Van der Waals Contacts. Small, 2021, 17, e2007739.	10.0	7
241	2D–1D mixed-dimensional heterostructures: progress, device applications and perspectives. Journal of Physics Condensed Matter, 2021, 33, 493001.	1.8	7
242	Encapsulating atomic molybdenum into hierarchical nitrogen-doped carbon nanoboxes for efficient oxygen reduction. Journal of Colloid and Interface Science, 2022, 620, 67-76.	9.4	7
243	Microstructure and mechanical property of Cu2O–Cu cermet prepared by in-situ reduction-hot pressing method. Materials Letters, 2008, 62, 3121-3123.	2.6	6
244	Microstructure evolution in hot deformation of 7050 aluminium alloy with coarse elongated grains. Materials Science and Technology, 2008, 24, 281-286.	1.6	6
245	Mössbauer spectrometry study of early stage spinodal decomposition in Fe–Cr–Co alloy under high magnetic field. Materials Letters, 2009, 63, 64-65.	2.6	6
246	Surfactant-free hydrothermal synthesis and characterization of single-crystal K2V8O21 nanobelts. Ceramics International, 2010, 36, 1825-1829.	4.8	6
247	Phase field simulation of spinodal decomposition under external magnetic field. Journal of Magnetism and Magnetic Materials, 2010, 322, 978-986.	2.3	6
248	Effect of microstructure on the electromagnetic properties of Al18B4O33w/Co and Al18B4O33w/FeCo composite particles. Journal of Applied Physics, 2012, 112, 053917.	2.5	6
249	Synthesis and electromagnetic properties of Fe/SiO 2 yolk/shell nanospheres with improved oxidation resistance. Micro and Nano Letters, 2013, 8, 349-352.	1.3	6
250	Adhesion and electronic structures of Cu/Zn2SnO4 interfaces: A first-principles study. Journal of Applied Physics, 2019, 125, .	2.5	6
251	Flaky FeSi particles with tunable size, morphology and microstructure developing for high-efficiency and broadband absorbing materials. Journal of Magnetism and Magnetic Materials, 2021, 527, 167800.	2.3	6
252	Jerky flow behavior in a rapid solidification processed Al–Li alloy. Materials Science & Engineering A: Structural Materials: Properties, Microstructure and Processing, 1998, 248, 221-229.	5.6	5

#	Article	IF	CITATIONS
253	Permeability calculation in composite media with low filler concentration: A new method of effective media theory application. Journal of Applied Physics, 2009, 105, 07A526.	2.5	5
254	Effect of Bi2Ti2O7 Seeding Layer on Capacitance-voltage Properties of Bi3.54Nd0.46Ti3O12 Films. Journal of Materials Science and Technology, 2010, 26, 206-210.	10.7	5
255	Aqueous solution synthesis and photoluminescence properties of two-dimensional dendritic PbWO4 nanostructures. Materials Research Bulletin, 2014, 56, 1-7.	5.2	5
256	Topochemical synthesis of ultrathin nanosheet-constructed Fe3O4 hierarchical structures as high-performance anode for Li-ion batteries. Journal of Materials Science: Materials in Electronics, 2018, 29, 7805-7810.	2.2	5
257	Few-layer WSe2 lateral homo- and hetero-junctions with superior optoelectronic performance by laser manufacturing. Science China Technological Sciences, 2020, 63, 1531-1537.	4.0	5
258	Charge Transfer at the Heteroâ€Interface of WSe <sub>2</sub> /InSe Induces Efficient Doping to Achieve Multiâ€Functional Lateral Homoâ€Junctions. Advanced Electronic Materials, 2021, 7, 2100584.	5.1	5
259	Impact fracture of rapid solidification processed Al-Li alloys. Materials Science & Engineering A: Structural Materials: Properties, Microstructure and Processing, 1996, 207, 87-96.	5.6	4
260	Effect of quenching rate on microstructures of a NiAl alloy. Materials Letters, 2001, 48, 121-126.	2.6	4
261	Through-Thickness Microstructure, Texture and Strength Gradients in AA 7055 Rolled Plate. Materials Science Forum, 2007, 546-549, 957-960.	0.3	4
262	High Temperature Deformation Mechanism of 7075 Aluminum Alloy. Key Engineering Materials, 2007, 353-358, 691-694.	0.4	4
263	Template-free Hydrothermal Preparation of Mesoporous TiO2 Microspheres on a Large Scale. Chemistry Letters, 2008, 37, 938-939.	1.3	4
264	Microstructure and electromagnetic properties of Al18B4O33w/Co composite particles prepared by electroless plating method. Surface and Coatings Technology, 2009, 203, 2221-2228.	4.8	4
265	Hyperfine structure variations in an Fe–Cr–Co alloy exposed to electron irradiation: Mössbauer spectroscopy characterization. Nuclear Instruments & Methods in Physics Research B, 2014, 338, 52-55.	1.4	4
266	Vertical aligned V2O5 nanoneedle arrays grown on Ti substrate as binder-free cathode for lithium-ion batteries. Ionics, 2017, 23, 2961-2967.	2.4	4
267	Topotactic Growth of Free-Standing Two-Dimensional Perovskite Niobates with Low Symmetry Phase. Nano Letters, 2021, 21, 4700-4707.	9.1	4
268	Data mining and design of electromagnetic properties of Co/FeSi filled coatings based on genetic algorithms optimized artificial neural networks (GA-ANN). Composites Part B: Engineering, 2021, 226, 109383.	12.0	4
269	Effects of Ga on the structural stability of Sm2(Fe,Ga)17 compounds. Materials Letters, 2002, 57, 146-150.	2.6	3
270	Effect of porosity and copper content on compressive strength of Cu/Cu2O cermet. Journal of Materials Science, 2004, 39, 731-732.	3.7	3

#	Article	IF	CITATIONS
271	Design of a two-layer ultra-wideband microwave absorber. , 2010, , .		3
272	Synthesis of lamellar niobic acid nanorods via proton-exchange and their conversion to T-Nb2O5 nanorods. Ceramics International, 2012, 38, 861-865.	4.8	3
273	THE NEGATIVE EFFECT OF NON-NBT PHASE ON THE FERROELECTRIC PROPERTIES OF SR-DOPED NBT THIN FILM AND THE SOLUTIONS. Surface Review and Letters, 2013, 20, 1350012.	1.1	3
274	Design, Fabrication and Characterization of Pressure-Responsive Films Based on The Orientation Dependence of Plasmonic Properties of Ag@Au Nanoplates. Scientific Reports, 2017, 7, 1676.	3.3	3
275	Enhanced photocatalytic activity and photoelectrochemical performance of InOOH nanosheets prepared via a facile solvothermal route. Journal of Materials Science: Materials in Electronics, 2017, 28, 1869-1876.	2.2	3
276	Charge Transport Behavior and Ultrasensitive Photoresponse Performance of Exfoliated F 16 CuPc Nanoflakes. Advanced Optical Materials, 2019, 7, 1901097.	7.3	3
277	Boosting the rate and cycling performance of $\hat{l}^2$ -Li V2O5 nanorods for Li ion battery by electrode surface decoration. Applied Surface Science, 2020, 512, 145622.	6.1	3
278	Effect of Pre-Stretch on the Precipitation Behavior and the Mechanical Properties of 2219 Al Alloy. Materials, 2021, 14, 2101.	2.9	3
279	Microstructure Analysis and the Effect of Cr Additive on Electrical Performance of (Cp-Nb)/Cu-Cd Electrical Contact Materials. , 2006, , .		2
280	Mechanical properties and oxidation behavior of the Ti–24Al–14Nb–3V–0.5Mo alloy sheet. Materials Science & Engineering A: Structural Materials: Properties, Microstructure and Processing, 2006, 427, 42-50.	5.6	2
281	The Contact Resistance and Arc Erosion Behavior of Separable C <sub>P</sub> -Nb-Cr/Cu-Cd Electrical Contact Material. Key Engineering Materials, 2007, 353-358, 886-889.	0.4	2
282	Grain characterization of nanostructured TiN coatings prepared by reactive plasma spraying. Surface and Interface Analysis, 2007, 39, 832-835.	1.8	2
283	Deformed Microstructure of AZ91 Magnesium Alloy Impacted by Projectiles with Velocities of 2-3 km/s. Journal of Solid Mechanics and Materials Engineering, 2010, 4, 720-726.	0.5	2
284	High strain rate superplasticity of TiN <sub>P</sub> /2014Al composite. Materials Science and Technology, 2011, 27, 670-675.	1.6	2
285	Edge treatment for sidelobe reduction of parabolic reflector antenna with a two-layer absorber. , 2011, , .		2
286	Formation of tubular BaTiO3 nanoparticle assembly through the Kirkendall effect using Na2Ti3O7 nanowires as template. Materials Research Bulletin, 2013, 48, 4565-4569.	5.2	2
287	Preparation of LSM-Nano-Film via a Water-Based Impregnation Process and Its Application onto Porous LSCF Cathode. Journal of the Electrochemical Society, 2013, 160, F905-F909.	2.9	2
288	STUDY OF THE NON-NBT PHASE IN <font>Sr</font> DOPED NBT THIN FILMS. Surface Review and Letters, 2013, 20, 1350056.	1.1	2

#	Article	IF	CITATIONS
289	9 Percolation in disordered conductor/insulator composites. , 2017, , 440-467.		2
290	Precipitation during Quenching in 2A97 Aluminum Alloy and the Influences from Grain Structure. Materials, 2021, 14, 2802.	2.9	2
291	Influence of aging on the impact fracture behavior of a RSP Al-Li alloy. Scripta Metallurgica Et Materialia, 1994, 30, 529-533.	1.0	1
292	Hydrogen induced fracture in a RSP Alî—,Li alloy. Scripta Metallurgica Et Materialia, 1994, 31, 595-599.	1.0	1
293	Effect of Original Microstructure on the Hot Compression Behavior of Superalloy 718. Key Engineering Materials, 2007, 353-358, 515-518.	0.4	1
294	XMCD study of Fe–Cr–Co alloy under electron irradiation. Journal of Electron Spectroscopy and Related Phenomena, 2010, 180, 34-38.	1.7	1
295	Preparation, microstructure, and electromagnetic properties of Al18B4O33w/CoxFeyBz composite powders. Surface and Coatings Technology, 2012, 212, 14-19.	4.8	1
296	Decorated membrane resonators as underground seismic wave barriers against high magnitude earthquakes. Journal of Applied Physics, 2020, 128, 084902.	2.5	1
297	An underground barrier of locally resonant metamaterial to attenuate surface elastic waves in solids. AIP Advances, 2020, 10, 075121.	1.3	1
298	In-situ tensile observation of a RSP Al-Li alloy in transmission electron microscope. Scripta Metallurgica Et Materialia, 1994, 30, 457-461.	1.0	0
299	Synthesis and Characterization of Single-Crystalline Alkali Titanate Nanowires ChemInform, 2005, 36, no.	0.0	0
300	Study of a Ceramic Thermocouple for Al Production. Materials Science Forum, 2007, 546-549, 2195-2198.	0.3	0
301	Dynamic Restoration Process of 7050 Aluminum Alloy during Superplastic Deformation. Key Engineering Materials, 2007, 353-358, 643-646.	0.4	0
302	DRX in 7050 Aluminum Alloy during Constraint Deformation Processing at High Temperature. Key Engineering Materials, 2007, 353-358, 647-650.	0.4	0
303	Texture Development during Cold and Cryogenic Rolling in AA 7055 Aluminum Alloy. Key Engineering Materials, 0, 353-358, 639-642.	0.4	0
304	High Strain Rate Superplastic Deformation Behavior of TiN <sub>P</sub> /2014Al Composite. Advanced Materials Research, 0, 97-101, 1633-1636.	0.3	0
305	Effect of microstructure on electromagnetic properties of ferromagnetic/dielectric composite particles. , 2010, , .		0
306	Effect of Hot Rolling Deformation on Superplastic Deformation Behavior of TiN <sub>P</sub> /2014Al Composite. Advanced Materials Research, 0, 264-265, 90-95.	0.3	0

#	Article	IF	CITATIONS
307	A Novel Ceramic Thermocouple Used in High-Temperature Measurement. Advanced Materials Research, 2011, 197-198, 328-332.	0.3	0
308	2D Materials: Electrochemical Intercalation in Atomically Thin van der Waals Materials for Structural Phase Transition and Device Applications (Adv. Mater. 6/2021). Advanced Materials, 2021, 33, 2170043.	21.0	0
309	Microstructures and Magnetic Properties of Single-Step Deposited Ce:YIG/YIG Bilayer Films With Different Layer Thickness Ratios. IEEE Transactions on Magnetics, 2022, 58, 1-5.	2.1	Ο